# Preliminary Study of Machine Learning Aided CFD Network to Reduce Computational Cost

Joongoo Jeon [a], Juhyeong Lee [a], Sung Joong Kim[a,b*]
[a] *Department of Nuclear Engineering, Hanyang University,*
[b]*Institute of Nano Science & Technology, Hanyang University*
*222 Wangsimni-ro, Seongdong-gu, Seoul 04763, Republic of Korea*
[*]*Corresponding author: sungjkim@hanyang.ac.kr*

## 1. Introduction

The regulatory requirement for severe accident management strategies has been evaluated at the system analysis code level [1]. The system analysis codes, like MELCOR code, have obvious strengths which can analysis the thermal hydraulic behavior in an entire reactor coolant system over extended periods of time. However, these codes cannot explicitly model the three-dimensional fluid behavior which can significantly affect the accident progress. There is an example of calculating the inlet plenum mixing fraction and recirculation ratio using the computational fluid dynamics (CFD) code as documented in NUREG-1781 [2]. It means that CFD codes will be used more actively in regulatory research.

Despite the improvement in computer performance, it is still difficult to simulate extended time with CFD simulation requiring fine grid and small timestep. This is especially true for turbulent or reacting flow accompanied by less than $mm$ and $ms$ scale [3, 4]. For this reason, research on CFD acceleration skill is a remaining issue to advance regulatory technology.

Since Rechenberg's evolutions strategy, machine learning has been applied to fluid dynamics. Recently, there are many data driven studies to predict the CFD variable fields of next timestep by previous fields. However, they noted that it is still difficult to predict multistep flow field due to error accumulation [5]. In this study, we proposed a novel concept of machine learning framework to enhance the CFD calculation speed. To investigate the feasibility of the framework, the accuracy of the machine learning aided CFD simulation was evaluated with the tier-derivative system based neural network.

## 2. Construction of CFD datasets

### *2.1 Modeling and Simulation*

To evaluate the accuracy of the machine learning aided CFD simulation, the datasets from CFD simulation was needed. In this study, CFD datasets were constructed from results of a stabilized hydrogen flame simulation (5.0 vol%) by using the ANSYS Fluent 18.0 code. Because this study was an early step of machine learning performance evaluation, the case study on laminar flame was carried out. The Fluent-CHEMKIN solver was particularly developed to couple the fluid dynamics with chemical combustion reactions. Investigation of the lean hydrogen flame is an essential part of the containment safety analysis. Especially, the stabilized flame analysis is vigorously being performed to evaluate the unique flammable limit of each mixture condition and compare the flame characteristics according to each concentration.

**Fig. 1** shows the computational domain which is an axisymmetric geometry with a height of 100 mm and a diameter of 25 mm. The modeled geometry is the same size to that used in our previous study observing the flame extinction of stretched hydrogen flames [4]. Unlike the previous study, the transient solver was used to produce the 5.0 vol% hydrogen flame CFD datasets over time (1 $ms$ timestep).

The species transport model, which can calculate the mixing and transport of chemical species by solving a conservation equation describing convection, diffusion, and detailed chemical kinetics, was used to examine the flame structure in the micro-region. The radiative transfer equation was solved using the discrete ordinates (DO) radiation model that solves the radiative heat transfer for a finite number of discrete solid angles. The DO radiation model is known to cover the entire range of optical thicknesses. The absorption coefficient of each cell was calculated by using the weighted-sum-of-gray-gases (WSGG) model [6].

The wall boundary condition was considered non-slip and isothermal because only a slight increase in wall temperature was observed in the experiments [7]. The mesh was uniformly structured to a size of 0.1 mm × 0.1 mm through the mesh sensitivity studies with a benchmarking simulation [8] (**Fig. 1**). The detailed modelling and validation results can be found in Ref [4].

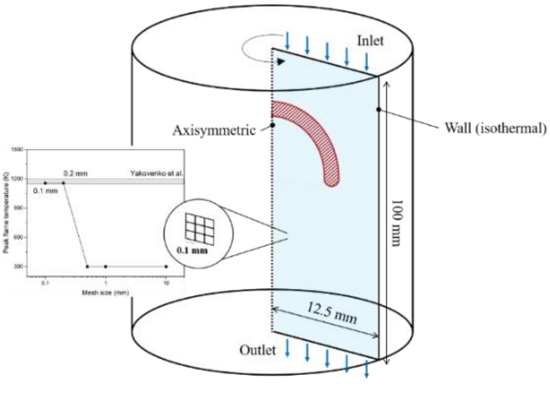

**Fig. 1.** Axisymmetric cylindrical domain and boundary conditions for 5.0 vol% hydrogen flame CFD datasets.

### *2.2 Datasets*

The datasets for this preliminary study consisted of a partial timeline within the entire simulation timeline. The entire timeline for stabilized flame generation process was depicted in **Fig. 2**. At 0 s before ignition, the temperature of all domain is 300 K. In 0.05s, the temperature and flame propagate out of the ignition area by the occurrence of ignition. The flame continues to expand until 0.5 s when the ignition energy is in effect. After 0.5 s, the flame begins to stabilize through the balance of heat loss mechanisms (conduction, radiation, convection) and combustion heat generated by the existing flame. This flame stabilizing period was selected as the subject of this study, hence the simulation results on the 0.600-0.605 timeline was used as datasets. Specifically, the results on 0.600-0.601 were used as training/validation sets and 0.601-0.605 were used as test sets. Methodology verification through extended timeline is our future works.

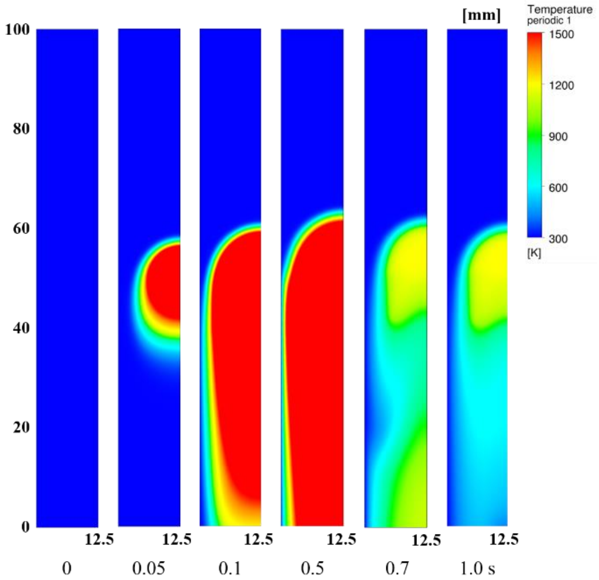

**Fig. 2.** Overall stabilized flame generation process from 0 to 1 sec by CFD temperature fields.

From the selected timeline of CFD results, variables to be used for neural network training and prediction was determined. **Fig. 3** shows the instantaneous variable fields for machine learning at timestep $t$. The variables used to learning machine was consists of flow variables $v_x, v_z$ and temperature variables $T$, and species variables $X_{H_2}, X_{H_2O}, X_{O_2}$ . More specifically, the data series in timestep $t$ were used as input, and the data series in timestep $t+1$ were used as output during training/prediction. The detailed input/output system will be described in *Section 3.4*.

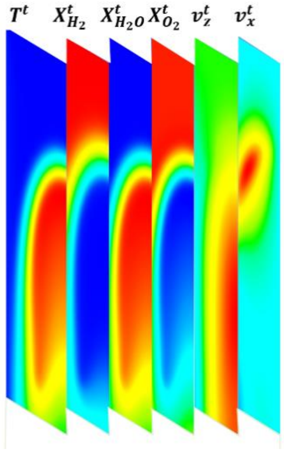

**Fig. 3.** Instantaneous fields of flow variables $v_x, v_z$ and temperature variables $T$, and species variables $X_{H_2}, X_{H_2O}, X_{O_2}$.

## 3. Machine learning methodology

### *3.1 Concept of Machine Learning aided CFD Network*

**Fig. 4** shows our novel concept of machine learning aided CFD network. It was noted that each of CFD and machine learning is not utilized alone, but the network is a combination form of both tools. The calculation of CFD alone has the limitations of the aforementioned computational cost, and the Machine learning alone cannot be free from error accumulation. The principle of the machine learning aided CFD network (MACnet) is to continuously update the parameters (weight, bias) of the neural network through CFD simulation at the connection point.

The machine (neural network) trained by the CFD results of timestep $t$ and $t+1$, predicts the CFD results of timestep from $t+2$ to $nt$. The prediction of the variable fields over single timestep is called multistep times series prediction. When the residual of the CFD results predicted by machine learning reaches a certain value, CFD simulation is performed again to obtain new parameters. For successful implementation of the MACnet, sufficient research on the loss function during training and prediction should be conducted. This is our future study. In this study, the feasibility of multistep time series prediction by single parameter update was investigated.

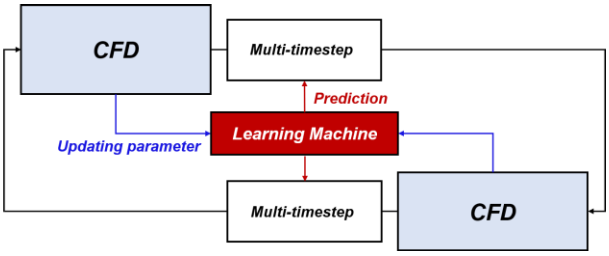

**Fig. 4.** Concept of machine learning aided CFD network with sequential parameter updating.

### *3.2 Procedure of machine learning for preliminary study: multistep time series prediction*

**Fig. 5** shows the procedure of machine learning in this study. After the simulation by Fluent code, the data preprocessing of the CFD results is required to transform them into a suitable matrix form for neural network training as shown **Eq. (2)**. Finally, neural network trained by the preprocessed CFD results predicted the variable fields for next timestep. Because this study aimed to predict the variable fields through single parameter update, the machine learning results were not used for CFD simulation again.

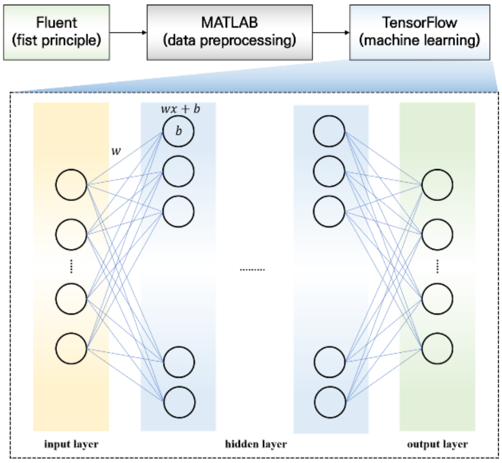

**Fig. 5.** Procedure of machine learning aided CFD simulation with single parameter update.

### *3.3 Configuration of neural network*

In this study, the accuracy of simple structured neural network to predict CFD variable fields was evaluated. **Table I** shows the important properties of the neural network model. Single hidden layer with 64 neurons composes the network. The number of inputs and outputs will be described in *Section 3.4*.

To minimize the mean square error (MSE) with the ground truth field (CFD), the Adam optimizer is used. **Eq. (1)** shows the gradient descent (GD) optimizer to determine weight and bias for each neuron. Gradient of loss function in each neuron $\nabla C$ can be calculated by the back propagation theory. The Adam optimizer (**Eq. (2)**), a kind of back propagation algorithm, was developed to enhance the computational speed of the GD optimizer. Where $w$ is updated parameter, is $m, v$ are moving average. $\eta, \beta$ is hyperparameters in machine learning. Both optimizers end up finding parameters to minimize the loss function through epochs (iterations). Iteration for parameter determination was repeated until no MSE reduction was observed for the 20% validation set.

Without an activation function, it is difficult to predict the nonlinear relationship between the input and output variables. As in the momentum equation of CFD code (**Eq. (3)**), the relationship between variables has non-linearity. For this reason, the ReLU activation function is used to introduce the non-linearity in the network.

**Table I:** Important properties of the neural network model

| Property | Feature (tier) |
|---|---|
| Number of inputs | 30 |
| Number of hidden layers | 1 |
| Neurons in hidden layer | 64 |
| Number of outputs | 1 |
| Loss function | mean square error |
| Activation function | ReLU |
| Optimizer | Adam |

$$\begin{bmatrix} w_1^{t+1} \\ w_2^{t+1} \\ \vdots \\ w_n^{t+1} \end{bmatrix} = \begin{bmatrix} w_1^{t} \\ w_2^{t} \\ \vdots \\ w_n^{t} \end{bmatrix} - \eta \nabla C = \begin{bmatrix} w_1^{t} \\ w_2^{t} \\ \vdots \\ w_n^{t} \end{bmatrix} - \eta \begin{bmatrix} \frac{\partial C}{\partial w_1^t} \\ \frac{\partial C}{\partial w_2^t} \\ \vdots \\ \frac{\partial C}{\partial w_n^t} \end{bmatrix} \tag{1}$$

$$\begin{bmatrix} w_1^{t+1} \\ w_2^{t+1} \\ \vdots \\ w_n^{t+1} \end{bmatrix} = \begin{bmatrix} w_1^{t} \\ w_2^{t} \\ \vdots \\ w_n^{t} \end{bmatrix} - \eta \begin{bmatrix} \frac{\frac{m_1^t}{1-\beta^t}}{\sqrt{\frac{v_1^t}{1-\beta'^t}}+\epsilon} \\ \frac{\frac{m_2^t}{1-\beta^t}}{\sqrt{\frac{v_2^t}{1-\beta'^t}}+\epsilon} \\ \vdots \\ \frac{\frac{m_n^t}{1-\beta^t}}{\sqrt{\frac{v_n^t}{1-\beta'^t}}+\epsilon} \end{bmatrix} \tag{2}$$

$$\frac{\partial}{\partial t}(\rho\vec{v}) + \nabla\cdot(\rho\vec{v}\vec{v}) = -\nabla p + \nabla\cdot(\bar{\bar{\tau}}) + \rho\vec{g} \tag{3}$$

### *3.4 Input/output systems for neural network*

We proposed a tier-derivative input/output system to imitate the first principles. In the finite volume method applied in CFD codes, the mass and heat transport between adjacent cells are calculated at every timestep. For this reason, we introduced a tier system to the neural network input. Each of the six variables of the cell and its 4 adjacent cells (2D geometry) used as inputs (**Table II**). In other words, a total of 30 (6 × 5) variable fields are used to predict 6 variable fields in the next timestep of each cell. The tier system was already proposed in previous works, but they simply set the outputs to the original values. However, the update of variables in the first principles process in a derivative form as shown **Eq. (3)**. For this reason, we combined the tier system with a derivative system for output (**Table II**). We expect that this increase in analogousness with the first principles can improve the machine learning performance along with a physics informed error function to be developed in future works.

**Table II:** Tier-derivative input/output system

| | Input (tier) | Output (derivative) |
|---|---|---|
| Flow | $\sum_1^5 v_{x,i}^t,\ v_{z,i}^t$ | $\frac{v_{x,1}^{t+1} - v_{x,1}^t}{\Delta t}$,<br>$\frac{v_{z,1}^{t+1} - v_{z,1}^t}{\Delta t}$ |
| Temperature | $\sum_1^5 T_i^t$ | $\frac{T_1^{t+1} - T_1^t}{\Delta t}$ |
| Species | $\sum_1^5 X_{H_2,i}^t, X_{O_2,i,}^t X_{H_2O,i}^t$ | $\frac{X_{H_2,1}^{t+1} - X_{H_2,1}^t}{\Delta t}$,<br>$\frac{X_{H_2O,1}^{t+1} - X_{H_2O,1}^t}{\Delta t}$,<br>$\frac{X_{O_2,1}^{t+1} - X_{O_2,1}^t}{\Delta t}$ |

## 4. Results and Conclusions

As described in *Section 2.2*, the CFD results on 0.600-0.601 was used as training/validation sets and 0.601-0.605 was used as test sets. In training of neural network, iteration for parameter determination was repeated until no MSE reduction was observed for the 20% validation set (number of epochs). After the training, the CFD results of 0.601 s were input to predict the variable fields of 0.602 s by machine learning. Then the 0.602 s variable fields were used to predict the 0.603 field, which was repeated until 0.605 s.

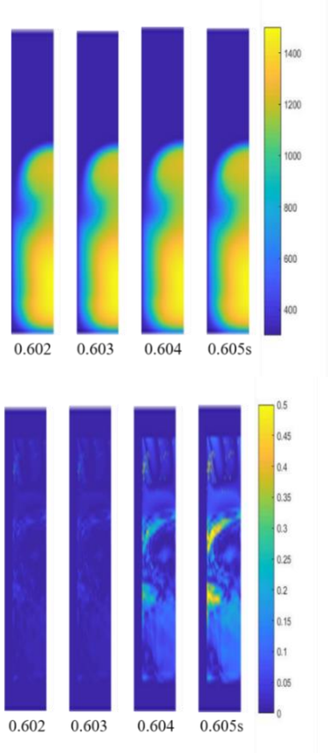

**Fig. 6.** Preliminary results of multistep time series prediction with the tier-derivative based neural network. **Upper**: temperature field ($K$), **lower**: error field (%).

In conclusion, **Fig. 6** shows the temperature and error field of multistep time series prediction from 0.600-0.605 s. The error field was depicted based on the absolute error between the CFD and machine learning results. It was identified that the results of the first two timesteps showed good agreement with the original CFD results, but the error increased from 0.604 sec. There were two important observations which can be made through the error field results. First, error accumulation became remarkable if the parameter update point and the prediction point get farther away. It was similar phenomena identified in previous studies [5]. Second, the local error increased near the flame front. It means that the machine learning also suffers from prediction difficulties in the stiff calculation region, as in the CFD simulation. In this study, the optimization of various elements constructing the neural network has not been sufficiently performed yet. Our future goal is to evaluate the performance of the MACnet for extended timeline through neural network improvement.

## Acknowledgement

This work was supported by the Nuclear Safety Research Program through the Korea Foundation of Nuclear Safety (KoFONS) using the financial resource granted by the Nuclear Safety and Security Commission (NSSC) of the Republic of Korea (grant number 2003006-0120-CG100).

## REFERENCES

[1] W. Choi, H.Y. Kim, R.J. Park, S. J. Kim, Effectiveness and adverse effects of in-vessel retention strategies under a postulated SGTR accident of an OPR1000, J. Nucl. Sci. Technol. (2017) 1-11.

[2] C. Boyd, K. Hardesty, CFD analysis of 1/7th scale steam generator inlet plenum mixing during a PWR severe accident, NUREG-1781, 2003.

[3] J. Jeon, Y. S. Kim, W. Choi, S. J. Kim, Identification of Hydrogen Flammability in steam generator compartment of OPR1000 using MELCOR and CFX codes, Nucl. Eng. Technol. 51 (2019) 1939-1950.

[4] J. Jeon, D. Shin, W. Choi, S.K. Kim. Identification of the extinction mechanism of lean limit hydrogen flames based on recirculation heat transfer, Int. J. Heat Mass Trans, In press.

[5] S. Lee, D. You, Data-driven prediction of unsteady flow over a circular cylinder using deep learning, J. Fluid Mech. 879 (2019) 217-254.

[6] Y. Shoshin, L. Tecce, J. Jarosinski, Experimental and computational study of lean limit methane-air flame propagating upward in a 24 mm diameter tube, Combust. Sci. Technol. 180 (2008) 1812-1828.

[7] F.E. Hernández-Pérez, B. Oostenrijk, Y. Shoshin, J.A. van Oijen, L.P. de Goey, Formation, prediction and analysis of stationary and stable ball-like flames at ultra-lean and normal-gravity conditions, Combust. Flame 162 (2015) 932-943.

[8] I. Yakovenko, M. Ivanov, A. Kiverin, K. Melnikova, Large-scale flame structures in ultra-lean hydrogen-air mixtures, Int. J. Hydrog. Energy 43 (2018) 1894-1901.